# Dalton Transactions

Accepted Manuscript






ROYAL SOCIETY OF CHEMISTRY

www.rsc.org/dalton

Cite this: DOI: 10.1039/c0xx00000x

www.rsc.org/xxxxxx

ARTICLE TYPE

# Polyaniline shell cross-linked $Fe_3O_4$ magnetic nanoparticles for heat activated killing of cancer cells

**Suman Rana,[a] Neena V. Jadhav,[b] K. C. Barick,*[,a] B. N. Pandey,[b] P. A. Hassan*[,a]**

***Received (in XXX, XXX) Xth XXXXXXXXX 20XX, Accepted Xth XXXXXXXXX 20XX***

**DOI: 10.1039/b000000x**

Superparamagnetic $Fe_3O_4$ nanoparticles are appealing materials for heat activated killing of cancer cells. Here, we report a novel method to enhance the heat activated killing of cancer cells under AC magnetic field (AMF) by introducing polyaniline impregnated shell onto the surface of $Fe_3O_4$ nanoparticles. These polyaniline shell cross-linked magnetic nanoparticles (PSMN) were prepared by *in-situ* polymerization of aniline hydrochloride on the surface of carboxyl PEGylated $Fe_3O_4$ nanoparticles. XRD and TEM analysis revealed the formation of single phase inverse spinel $Fe_3O_4$ nanoparticles of size about 10 nm. The successful growth of polyaniline shell on the surface of carboxyl PEGylated magnetic nanoparticles (CPMN) is evident from FTIR spectra, DLS, TGA, zeta-potential and magnetic measurements. Both CPMN and PSMN show good colloidal stability, superparamagnetic behavior at room temperature and excellent heating efficacy under AMF. It has been observed that the heating efficacy of PSMN under AMF slightly reduced as compared to that of CPMN. The enhanced toxicity of PSMN to cancer cells under AMF suggests their strong potential for magnetic hyperthermia. Further, PSMN shows high loading affinity for anticancer drug (doxorubicin), its sustained release and substantial internalization in tumor cells.

## Introduction

Recently, there has been immense interest in the fabrication of multifunctional nanostructures due to their unique and tunable physio-chemical properties for various biomedical applications.[1,2] It is important to modify the surface of these nanostructures with suitable functionalities such as reactive organic or inorganic moieties, proteins, polymers etc. for enhanced stability and biocompatibility. Amongst others, there has been a growing interest in fabrication of polymer coated magnetic nanostructures as contrast agents for magnetic resonance imaging (MRI), heat activated killing of cancer cells (so-called hyperthermia therapy) and targeted drug delivery.[3-6] The magnetic component is responsible for enhanced contrast in MRI, magnetic field induced heating and site specific drug delivery. However, the polymer counterpart helps in tuning the magnetic response of particle as well as provides biocompatibility, colloidal stability and active sites for the conjugation of biomolecules, receptors and drugs etc. Thus, site-selective targeting and localized heating of cancer cells can be successfully achieved by using polymer shell cross-linked magnetic nanoparticles.[7-10]

Superparamagnetic $Fe_3O_4$ nanoparticles have been extensively used as a core material for hyperthermia due to their remarkable magnetic properties, low toxicity and good heat activation capacity in the presence of AMF.[11-14] It is well established that cancer cells are more sensitive to heat damage under hyperthermia condition compared to normal cells.[15] The effectiveness of any effort to treat cancer by hyperthermia is dependent on achieving good heating efficacy at low dose of particles and low frequency. In view of above, the polymer coating on $Fe_3O_4$ nanoparticles must afford colloidal and chemical stability in cellular medium while retaining their optimal magnetic properties for higher heating efficacy. Recently, new developments appeared in designing and synthesis of conducting polymer shell cross-linked magnetic nanoparticles.[16-19] Amongst others, conducting polymers such as polypyrrole and polyaniline have received special attention due to their unique π-conjugated structures, which lead to good environmental stability and high electrical conductivity. Bidan et al.[16] demonstrated an electrochemical method to fabricate core-shell nanostructure in which magnetic core is surrounded by anionic complexing polypyrrole shell. Deng et al.[17] reported the preparation of $Fe_3O_4$-polyaniline nanoparticles having core-shell nanostructure. Even though many materials and methods are developed for fabrication of conducting polymer shell cross-linked magnetic nanoparticles, their use in heat activated killing of cancer cells is not much studied.

Herein, we report the preparation of polyaniline impregnated shell cross-linked magnetic nanoparticles by a facile soft-chemical approach. Specifically, the excellent colloidal stability,

[a]*Chemistry Division, Bhabha Atomic Research Centre, Mumbai-400085, India. E-mail: kcbarick@barc.gov.in (K. C. Barick), hassan@barc.gov.in (P. A. Hassan);* Fax: *91 22 2550 5151*; Tel: *91 22 2559 5099*

[b]*Radiation Biology and Health Sciences Division, Bhabha Atomic Research Centre, Mumbai-400085, India*

†Electronic Supplementary Information (ESI) available: Details of cell culture and MTT assay, synthesis scheme, FTIR, UV-Vis., XRD, TGA, DLS, release profile, cell viability and laser induced heating, protein interaction (Fig. S1-S9, Table S1). See DOI: 10.1039/b000000x/

good self-heating efficacy, high loading affinity for anticancer drug and substantial internalization in tumor cells make these novel nanoparticles suitable for cancer therapy. It is interesting to mention that the polyaniline impregnated shell on magnetic nanoparticles enhances the heat activated killing of cancer cells under AMF.

## Materials and methods

Ferrous chloride tetrahydrate ($FeCl_2.4H_2O$), ferric chloride hexahydrate ($FeCl_3.6H_2O$), PEG-diacid (Poly (ethylene glycol) bis (carboxymethyl) ether, $M_n$ = 600), aniline hydrochloride, bovine serum albumin (BSA), doxorubicin hydrochloride (DOX) and thiazolyl blue tetrazolium bromide (MTT) were purchased from Sigma-Aldrich, USA. 25% ammonia solution and acetic acid were purchased from Thomas Baker Chemical Pvt. Ltd., India. Potassium peroxodisulfate and dimethyl sulfoxide (DMSO) were obtained from E. Merck (India) Ltd. and SD fine chemical Ltd., India, respectively. All chemicals are of analytical grade and used without further purification. The acetate buffer (AB)-pH 5 and phosphate buffered saline (PBS)-pH 7.3 were prepared using standard protocols.

The polyaniline shell cross-linked magnetic nanoparticles (PSMN) were synthesized by simple and facile two step process, carboxyl PEGylation of $Fe_3O_4$ nanoparticles followed by cross-linking of polyaniline shell on PEGylated particles. The carboxyl PEGylated $Fe_3O_4$ magnetic nanoparticles (CPMN) were synthesized through co-precipitation of Fe-chlorides precursors in aqueous medium followed by *in-situ* functionalization of PEG-diacid. In a typical synthesis, 1.988 g of $FeCl_2.4H_2O$ and 5.406 g of $FeCl_3$. $6H_2O$ were dissolved in 80 ml of water in a round bottom flask and temperature was slowly increased to 70 $^oC$ in refluxing condition under $N_2$ atmosphere with constant mechanical stirring at 1000 rpm. The temperature was maintained at 70 $^oC$ for 30 min and then 30 ml of 25% ammonia solution was added instantaneously to the reaction mixture, and kept for another 30 min at 70 $^oC$. Then, 5 ml PEG-diacid was added and temperature was slowly raised up to 90 $^oC$ under reflux and reacted for 60 min with continuous stirring. The obtained black colored CPMN were then thoroughly rinsed with water and separated from the supernatant using a permanent magnet.

In order to provide polyaniline shell, 12 ml of 0.1 M aniline hydrochloride was added to 20 ml aqueous suspension of CPMN (1 gm). This reaction mixture was thoroughly mixed under ultrasonic bath for 15 min followed by mechanical stirring for 30 min. Then, 4 ml potassium peroxodisulfate (0.04 M) was added to initiate the polymerization process and reaction was allowed to proceed for 2 h under vigorous stirring. The products were thoroughly rinsed with water and separated from solution using a permanent magnet, and purified by dialysis against milli Q water.

X-ray diffraction (XRD) pattern was recorded on a Phillips PW1710 diffractometer with Cu Kα radiation. The crystallite size is estimated from the X-ray line broadening using Scherrer formula. The infrared spectra were recorded in the range 400-4000 $cm^{-1}$ on a Fourier transforms infrared spectrometer (FTIR, Bomen Hartman and Braun, MB series). The transmission electron micrograph was taken by Philips CM 200 TEM for particle size determination. The thermogravimetric analysis (TGA, Setaram Instrumentation) was performed under $N_2$ atmosphere from room temperature to 650 $^oC$ with a heating rate of 10 $^oC$/min. Dynamic light scattering (DLS) measurements were performed using a Malvern 4800 Autosizer employing a 7132 digital correlator for the determination of hydrodynamic diameter. The zeta-potential measurements were determined by Zetasizer nano series, Malvern Instruments. The field dependent magnetization measurements were carried out by physical property measurement system (PPMS, Quantum Design). The concentration of Fe in suspensions was obtained by phenanthroline spectrophotometric method.[20] The colloidal stability was investigated by measuring the change in absorbance of sample suspensions (0.1 mg/ml) in different medium at 350 nm using JASCO V-650, UV-visible spectrophotometer.

The heating ability of sample suspensions was obtained from the time-dependent calorimetric measurements using an induction heating unit. 1 ml of sample suspensions of different concentrations of Fe (0.5, 1 and 2 mg/ml) was taken in an eppendorf with suitable arrangements to minimize the heat loss. The AMF of 0.335 kOe and frequency of 265 kHz were used to evaluate the specific absorption rate (SAR). The SAR was calculated as follows[11]:

$$\mathrm{SAR} = C\frac{\Delta T}{\Delta t}\frac{1}{m_{\mathrm{Fe}}}$$

where $C$ is the specific heat of solvent ($C = C_{\mathrm{water}}$ = 4.18 J/g °C), $\Delta T/\Delta t$ is the initial slope of the time-dependent temperature curve and $m_{\mathrm{Fe}}$ is mass fraction of Fe in the sample. The rise in temperature was also monitored using a high resolution infrared (IR) camera (Thermal Imager Testo 875-1), and analyzed by thermography software (Testo IR Soft Software, version 3.1).

The heat activated killing of cancer cells (mouse fibrosarcoma cells, WEHI-164) were evaluated under AMF with respective controls using the MTT assay. Cells ($0.25\times10^6$) were seeded overnight in petridishes (P-60) containing 4 ml culture medium (complete DMEM) followed by treatment with CPMN and PSMN (0.5 and 1 mg) for 3 h at culture conditions. Then, cultures were subjected to AMF (0.335 kOe) for 10 min under sterile conditions using induction heating unit. After AMF exposure, cells were further cultured for 48 h. Then, the media containing nanoparticles was carefully removed and processed for MTT assay to determine the cell viability (details of cell culture and MTT assay are provided in ESI†). Cells treated with different conditions are referred as follows: (i) control cells (C), (ii) cells with AMF only (C + H), (iii) particles only (0.5 and 1 mg) and (iv) cells treated with particles followed by exposure of AMF (0.5 mg + H, 1 mg + H).

The anticancer agent, doxorubicin hydrochloride (DOX) was used as a model drug to estimate the drug loading and release behavior of the PSMN. The loading was carried out by incubating 0.5 ml of aqueous solution of DOX (1 mg/ml) with 2.5 ml of the aqueous suspension of PSMN (2 mg/ml, pH 7.3) for 1h in dark. Drug loaded samples were separated from the free-standing drug molecules through magnetic separation and carefully washed with milli Q water. The pH-triggered drug release studies were carried out under reservoir (r) - sink (s) conditions (AB-pH 5 vs. AB pH-5, PBS-pH 7.3 vs. PBS-pH 7.3). The drug-loaded PSMN (5 mg) were immersed into 5 ml of pH 5/pH 7.3 and then put into a dialysis bag. The dialysis was performed against 200 ml of respective sink medium under

continuous stirring at 37°C to mimic the cellular environment. One ml of the external medium was withdrawn and replaced with fresh same medium at fixed interval of times to maintain the sink conditions. The amount of doxorubicin released was determined by measuring the fluorescence emission at 585 nm (excitation wave length: 490 nm) using a plate reader (Infinite M1000, Tecan-I control, Switzerland) against the standard plot prepared under similar condition. Each experiment was performed in triplicates and standard deviation was given in the plot.

Cellular uptake of DOX loaded PSMN was studied by confocal microscopy. For confocal microscopy imaging, cells (0.5 x $10^6$) were seeded on glass coverslips and cultured overnight. The cells were then treated with DOX-PSMN (10 μM DOX) for 3h at culture conditions, followed by washing with PBS. The cells were mounted on a glass slide in cell mounting medium (Invitrogen, USA) containing DAPI for nuclear staining. These cells were then imaged using confocal laser scanning microscopy (CLSM, LS510 Meta, Carl Zeiss, Germany). The excitation source used was an Ar ion laser (488 nm for DOX and 364 nm for DAPI) and emission window was set at 575-615 nm and 430-480 nm for DOX and DAPI, respectively. Further, the killing of cancer cells in presence of DOX-PSMN under AMF was evaluated with respective controls using the MTT assay as mentioned before.

The hemolysis assay and protein-particle interaction study were performed to evaluate the hemocompatibility (with human whole blood) and protein resistance characteristic (with BSA) of PSMN, respectively as reported elsewhere.[11]

## Results and discussion

Polyaniline shell was grown on PEG diacid functionalized $Fe_3O_4$ nanoparticles by polymerization reaction as described in the Scheme 1. First, the functionalization of $Fe_3O_4$ nanoparticles with PEG diacid (carboxyl PEGylation) was carried out *in-situ* during co-precipitation of $Fe^{2+}$ and $Fe^{3+}$ ions in basic medium. FTIR spectroscopic studies of CPMN indicate that PEG diacid is chemisorbed onto the surface of $Fe_3O_4$ nanoparticles through one carboxylate ions ($COO^-$) leaving the other one free on the surface (Fig. S1, ESI†). These CPMN were chosen as the core material for further fabrication of polyaniline shell due to their high negative surface charge (discussed later) and good aqueous colloidal stability (Fig. S2, ESI†). Further, it is well reported that PEGylated nanoparticles are more biodegradable, less antigenic, and non-irritating for tissues and less toxic than unmodified nanoparticles.[21] At the same time, the PEG chains are responsible for the so-called "stealth effect", preventing non-specific adsorption of opsonin proteins.[22]

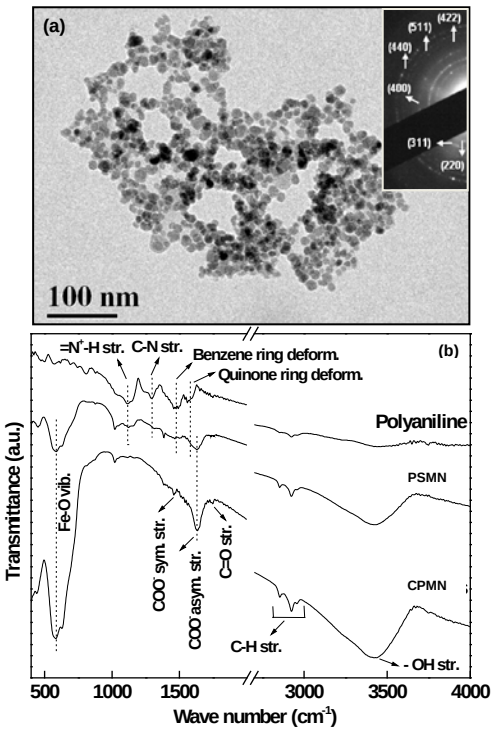


Fig. 1. (a) TEM image of PSMN (inset shows its electron diffraction pattern) and (b) FTIR spectra of polyaniline, CPMN and PSMN with their peak assignments (pure polyaniline is prepared by similar method in absence of $Fe_3O_4$ nanoparticles for comparative purpose).

The XRD patterns of CPMN and PSMN (Fig. S3, ESI†) reveal the formation of highly crystalline single phase cubic inverse spinel $Fe_3O_4$ nanostructure with an average crystallite size of about 10 nm (σ<10 %). The broad peak representing the periodicity parallel to the polymer chains of PEG and polyaniline were not clearly observed at 2θ around 25° due to the weak

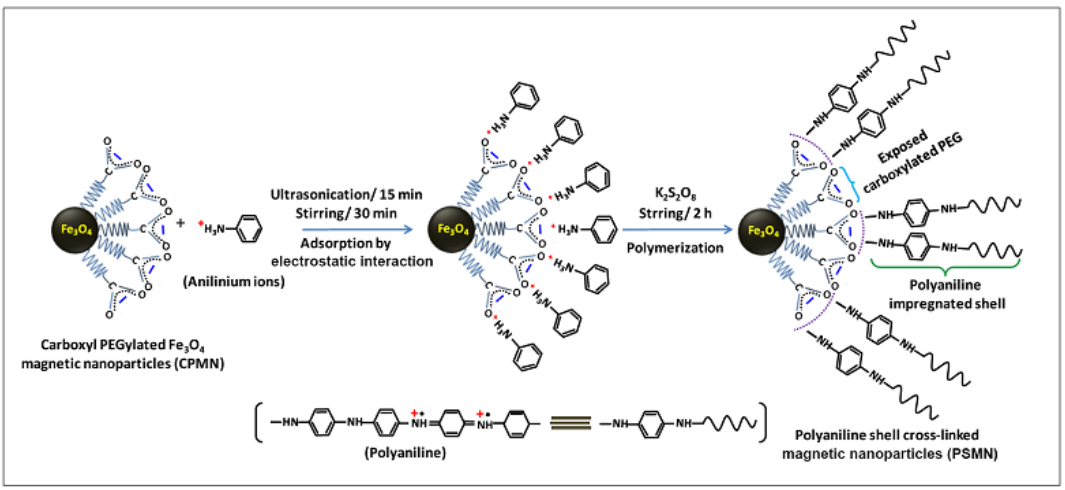


Scheme 1. Schematic representation of growth of polyaniline shell on PEGylated $Fe_3O_4$ nanoparticles by polymerization reaction.

intensity in comparison to the intense diffraction peaks of $Fe_3O_4$. The lattice constant was found to be ~8.379 Å, which is very close to the reported value of magnetite (JCPDS Card No. 88-0315, a = 8.375 Å). From TEM micrographs of PSMN (Fig. 1a), it is evident that $Fe_3O_4$ nanoparticles are almost spherical in shape with an average size of ~10 nm. The electron diffraction pattern (inset of Fig. 1a) of PSMN also confirmed the high crystallinity of nanoparticles. The electron diffraction pattern can be indexed to (220), (311), (400), (422), (511) and (440) reflections of cubic inverse spinel $Fe_3O_4$ structure, which is consistent with the XRD result.

The polyaniline shell cross-linking on the surface of CPMN was investigated by FTIR, DLS, zeta-potential and TGA analysis. Fig. 1b shows the FTIR spectra of polyaniline, CPMN and PSMN with their peak assignments. The vibrational bands for the polyaniline are well resolved, but those of the PSMN are rather broad and few. Specifically, the appearance of vibrational modes of quinone ring deformation, benzene ring deformation and C-N stretching of a secondary aromatic amine at 1575, 1480 and 1293 $cm^{-1}$, respectively in the FTIR spectrum of PSMN with slight shifting of band position clearly suggest the successful polymerization of polyaniline onto the surface of the CPMN.[23,24] Furthermore, the appearance of $=N^+$-H stretching mode of polyaniline at about 1120 $cm^{-1}$ in FTIR spectra of PSMN indicate the existence of polyaniline in the form of emeraldine salt, which has high conductivity.[24]

The mechanism of formation of polyaniline shell on $Fe_3O_4$ nanoparticles through *in-situ* polymerization can be explained by invoking an interfacial polymerization process. First, the cationic anilinium ions are adsorbed onto the negatively charged CPMN surface in a close proximity through the formation of $–COO^{-}\cdots\cdots H_3N^{+}–$ ion pairs. This adsorption results in great increase of the local concentration of aniline monomer near the $Fe_3O_4$ core, which is favorable for the initial polymerization of aniline under low monomer concentration. Moreover, from surface energy considerations, heterogeneous nucleation of polyaniline nanoparticles at the CPMN surface is energetically favored than homogenous nucleation of polyaniline in the bulk solution. Once the polyaniline nuclei are generated, the polymerization takes place preferentially and continuously on the existing polyaniline on the surface of nanoparticles rather than in solution. Hence, the shell cross-linking via polymerization was successfully initiated, propagated and terminated on the surface of PEGylated $Fe_3O_4$ resulting a conducting polymer cross-linked nanostructure. In a similar type of study, Jang et al.[23] reported the synthesis of monodisperse silica-polyaniline core-shell nanoparticles by *in-situ* polymerization of aniline monomers adsorbed on the negatively charged silica surface through electrostatic interactions. However, in present study, one cannot negate the possibility of forming polyaniline impregnated PEG shell, rather than a well separated PEG-PANI interface. This can arise from various reasons such as conformational flexibility of PEG chains which allows penetration of PANI chains, low molecular weight oligomer formation due to low monomer content and formation of patchy PANI particles on the surface rather than uniform coating. We believe that such composite structure of PANI and PEG could be advantageous for the effective heat transport from $Fe_3O_4$ core to the surrounding medium. The poor electron density contrast between PEG and PANI does not permit identification of the exact microstructure at the PEG-PANI composite surface. The thermogravimetric analysis of PSMN shows a weight loss of about 7.9%, whereas that of CPMN was 4% (Fig. S4, ESI†). This result (higher weight loss) clearly supports the organic modification during the formation of polyaniline impregnated shell on the surface of CPMN. An increase in the molecular weight of the organic chains attached to the $Fe_3O_4$ nanoparticles, during the growth of the conducting polymer shell, is also manifested from DLS (Fig. S5, ESI†). DLS measurements indicate that both CPMN and PSMN show monomodal distribution with mean hydrodynamic diameter of 40 and 65 nm, respectively (polydispersity index ~ 0.2). The larger hydrodynamic diameter of PSMN is primarily due to the presence of associated and hydrated long chain organic layers.[13] As DLS is weighted towards large sizes, the average hydrodynamic diameter could be higher than those obtained from TEM. Further, the average hydrodynamic diameter and polydispersity index hardly varies with time revealing their excellent aqueous colloidal stability.

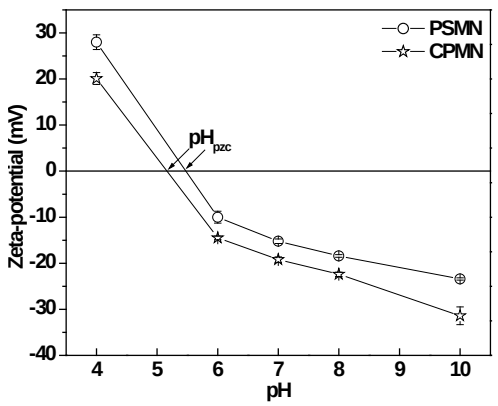


Fig. 2. Variation in the zeta-potential of CPMN and PSMN suspensions at different pH values (0.05 mg/ml).

Fig. 2 shows the variation in the zeta-potential of CPMN and PSMN suspensions at different pH values (0.05 mg/ml). From zeta-potential measurements, the isoelectric point (pH of zero point charge, $pH_{pzc}$) of CPMN and PSMN were found to be around 5.15 and 5.46, respectively. Thus, these nanoparticles have net positive surface charge at pH < $pH_{pzc}$ and negative surface charge at pH > $pH_{pzc}$. This reversal of charge property may be attributed to the different degree of ionization of functional groups at different pH values. Further, the increase in surface charge (at all measured pH) and shifting of isoelectric point towards higher pH value upon cross-linking of polyaniline shell is possibly due to the creation of positive charges ($=N^+$-H) on the surface of CPMN.[25] These results further suggest the grafting of polyaniline shell on the surface of PEGylated particles. The colloidal stability of the PSMN was also assessed from the changes in light scattering intensity as well as extinction changes with time. The insignificant change in absorbance of PSMN suspensions in aqueous and cell culture (complete DMEM) media indicates their good colloidal stability (Fig. S6, ESI†). These nanoparticles are hydrophilic in nature possibly due to the formation of hydrogen bonds between surface functional groups and water. In addition, the electrostatic repulsive force

originating from the ionization of the surface groups provide additional stability to the particles. Furthermore, the negative zeta-potential of CPMN and PSMN at physiological medium could decrease the possibility of their combination with hemoglobin, which would play an important role in improving the stability and blood compatibility.

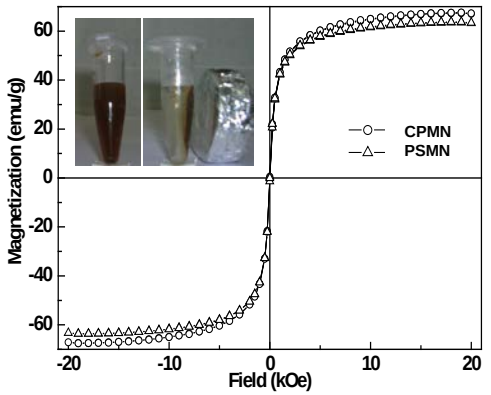


Fig. 3. Field dependent magnetization plots of CPMN and PSMN at 300 K (inset shows the photographs of PSMN in presence and absence of permanent magnet of field strength ~2.5 kOe).

In order to assess the potential of CPMN and PSMN in hyperthermia, we have investigated their magnetic and thermomagnetic properties. Fig. 3 shows the field dependent magnetization plots of CPMN and PSMN at 300 K. Both samples exhibit superparamagnetic behavior without magnetic hysteresis and remanence at 300 K. The maximum magnetizations were found to be 67.5 and 63.5 emu/g for CPMN and PSMN, respectively at 20 kOe. These low values of magnetization of both samples as compared to bulk $Fe_3O_4$ (92 emu/g) can be attributed to the combined effect of nano-sized $Fe_3O_4$ particles (large surface to volume ratio) and robust coating of non-magnetic organic moieties on their surface (quenching of magnetic moment by electron exchange between coating and surface atoms).[26] The low magnetization of PSMN as compared to CPMN is due to the grafting of polyaniline shell, which directly affects the crystallo-chemical properties of the magnetic nanoparticles surface and leads to an increase in the magnetically disordered surface layer. However, the retention of superparamagnetic property at room temperature with biocompatible organic shell makes these nanoparticles suitable as effective heating source for hyperthermia treatment of cancer cells.

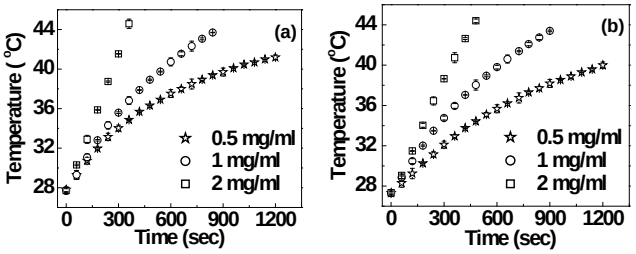


Fig. 4. Temperature *vs.* time plots of (a) CPMN and (b) PSMN at an applied field of 0.335 kOe.

Fig. 4 shows the temperature *vs.* time plots of (a) CPMN and (b) PSMN at an applied field of 0.335 kOe. They showed a time-dependent gradual increase in temperature of both CPMN and PSMN suspension. Our inductive heating experiments show that a magnetic field of 0.335 kOe at fixed frequency of 265 kHz is able to produce enough energy for raising the temperature of magnetic suspension at a concentration of 1 mg/ml of Fe to 43 °C (hyperthermia temperature) within 15 min. In thermal activation of superparamagnetic $Fe_3O_4$ nanoparticles under AC magnetic field, an increase in temperature is mainly due to the loss processes during the reorientation of the magnetization (Néel relaxation) or frictional losses with particle rotation in low-viscous environments (Brownian relaxation).[11,27] The Néel and Brownian relaxation times are given by the following equations:

$$\tau_B = \frac{4\pi\eta R_H^3}{k_B T}$$

$$\tau_N = \tau_0 e^{KV_M/k_B T}$$

$$\tau_{eff} = \frac{\tau_N \tau_B}{\tau_N + \tau_B}$$

where $\tau_B$ is the Brownian relaxation time, $\tau_N$ is the Néel relaxation time, $\tau_0 \approx 10^{-9}$ s, K is the anisotropy constant, $V_M$ is the volume of the $Fe_3O_4$ nanoparticle, $k_B$ is Boltzmann's constant, T is temperature, $\eta$ is the viscosity and $R_H$ is the hydrodynamic particle radius.

Table 1. The obtained SAR values of CPMN and PSMN suspensions along with their maximum magnetization ($M_{max}$) at 20 kOe.

| Magnetic suspensions | $M_{Max}$ (emu/g) | SAR (W/g of Fe) at different concentrations (in terms of Fe) under AMF of 0.335 kOe | | |
|---|---|---|---|---|
| | | 0.5 mg/ml | 1 mg/ml | 2 mg/ml |
| CPMN | 67.5 | 145 | 114 | 90 |
| PSMN | 63.5 | 120 | 100 | 80 |

The use of magnetic nanoparticles in thermal therapy depends on their heating efficiency, which is expressed in terms of specific absorption rate (SAR). The obtained SAR values of CPMN and PSMN suspensions are shown in Table 1 along with their maximum magnetization at 20 kOe. The observed good SAR is likely to be due to a combination of their strong magnetic responsivity and aqueous colloidal stability. It has been observed that SAR decreases with increasing the Fe concentration. This may be due to the decrease in Brownian contribution to hyperthermia and increase in magnetic dipole-dipole interactions between nanoparticles in suspension as a result of increase in local concentration. In addition, SAR is also dependent on various parameters such as applied field strength, magnitude of frequency and physical properties of magnetic particles.[11,28] Furthermore, it has been observed that the SAR values of PSMN are found to be slightly lower than those of CPMN at all concentrations, which is obvious as they possess less magnetic moments.

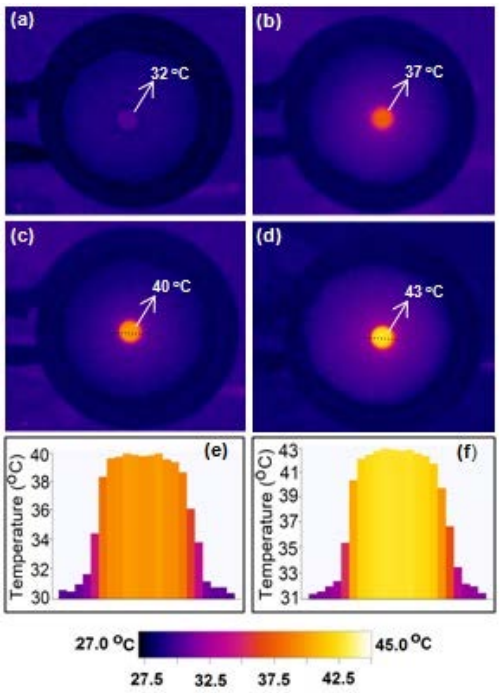


Fig. 5. (a-d) IR thermograms showing the rise in temperature of PSMN suspension during the exposure of AMF of 0.335 kOe (top view of samples) and (e, f) temperature distribution in PSMN suspension along the marked dotted line in Fig. 5 (c) and (d), respectively.

The rise in temperature was also visualized by the time dependant changes in IR thermograms (Fig. 5a-d). The central circle represents the PSMN suspension, which was heated by induction heating unit and demonstrates that the hyperthermia induced by the AMF selectively heated the specific area where the magnetic suspension was placed. The rise in temperature is clearly evident from the changes in colour of the central region of thermograms. The temperature profiles (Fig. 5e and f) along the sample zone (marked dotted line in Fig. 5c and d) clearly show a sharp decline in temperature at the periphery indicating localized heating of the specimen. This localized heating of magnetic suspension under AMF is necessary for *in-vitro* hyperthermia treatment of cancer cells.

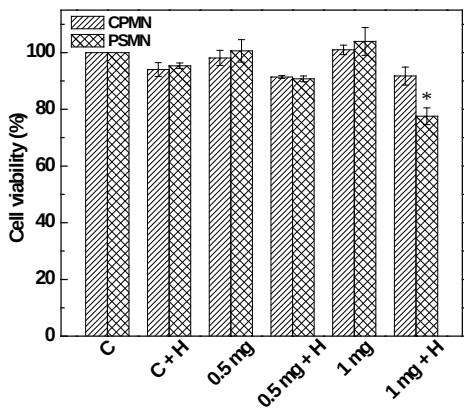


Fig. 6. Viability of WEHI-164 cells upon exposure of AMF (0.335 kOe) for 10 min in presence of CPMN and PSMN with respective controls. Data are presented as mean ± SD, *P<0.05.

Having noted the good heating efficacy of both CPMN and PSMN, we have also studied their hyperthermic tumor cell killing efficiency in WEHI-164 tumor cells in presence and absence of AMF (Fig. 6). It has been observed that the control cells (untreated) and cells treated with particles only (- hyperthermia) did not show significant change in the percentage cell viability. This indicates that both CPMN and PSMN have negligible cytotoxicity by itself. However, it is worth mentioning that PSMN under AMF (+ hyperthermia) showed about 22.5% decrease in cell viability for 1 mg of PSMN as compared to the marginal (~8%) decrease with CPMN under similar condition. This may be explained on the basis of the surface charge of these particles in culture medium. The zeta-potential of CPMN and PSMN in culture medium were found to be -15 and - 8 mV, respectively. The PSMN having higher surface charge (less negative) may have higher affinity for WEHI-164 cells as compared to CPMN. Recently, Motskin et al.[29] studied the uptake of negatively charged hydroxyapatite (HAP) nanoparticles by human monocyte-macrophage cells and observed that the HAP nanoparticles with higher zeta potential value (less negative) showed greater uptake. These cytotoxicity results were also supported by alterations in cellular morphology (cell detachment and circularization) and a decrease in cell number as visualized by optical microscopy (Fig. 7). From the images of cancer cells treated with 1 mg of PSMN and AMF (1 mg + H), it is evident that there is significant death of cells via apoptosis. However, further investigations are required to understand the exact mechanism of cell death by PSMN under exposure of AMF. Specifically, this study demonstrates the potential of polyaniline shell cross-linked $Fe_3O_4$ nanoparticles for hyperthermia treatment of cancer cells.

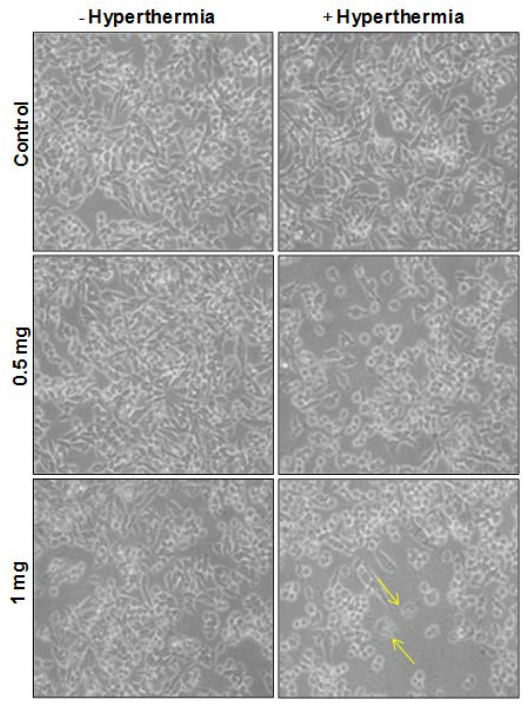


Fig. 7. Photographs of WEHI-164 cells taken 48 h after the treatment of PSMN with and without exposure of AMF (Magnification: 200 X). Arrows indicate the cells undergoing apoptosis.

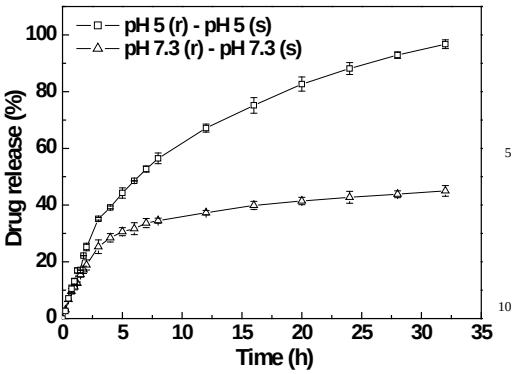


Fig. 8. pH dependent drug release profile of DOX-PSMN in cellular mimicking environment at 37 °C.

About 60% drug-loading efficiency (w/w) was obtained upon incubating 0.5 ml of aqueous solution of DOX (1 mg/ml) with 2.5 ml of the aqueous suspension of PSMN (2 mg/ml, pH 7.3) for 1h in dark at room temperature. Further, the zeta-potential of the PSMN (100 µg/ml suspension) increased from -24.0 mV to -5.0 mV upon incubating with an aqueous solution of 10 µg/ml of DOX. This increase in surface charge arises from the binding of cationic DOX (protonated primary amine present on the drug induces a positive charge) with negatively charged nanoparticles (PSMN) predominately through electrostatic interactions. The affinity of DOX for negatively charged molecules has been the subject of numerous earlier investigations .[14,30,31]

The release of drug molecules from DOX-PSMN (Fig. 8) follows a time dependent sustained release profile. Furthermore, the short time behavior (Fig. S7, ESI†) shows a linear relationship between the drug release and square root of time ($t^{1/2}$) as expected from Higuchi drug release model confirming that the DOX release process is diffusion-controlled.[32] It is interesting to observe from the release profiles that the release rate of DOX is higher at lower pH. This is desirable for cancer therapy as the relatively low pH in tumors will specifically stimulate the DOX release in the target site. The pH triggered release of DOX could be attributed to the weakening of the electrostatic interactions between the drug and PSMN.

The results obtained from drug release studies prompted us to explore the cellular uptake of PSMN by cancer cells. Fig. 9 shows the CLSM images of WEHI-164 cells after incubation with the DOX and DOX-PSMN at culture conditions. A significant uptake of DOX-PSMN was clearly observed from the red fluorescence image arising from DOX emissions, suggesting that the drug loaded nanoparticles were internalized in the cells. The blue fluorescence image shows emission from nucleus stained with DAPI. The merged image of DOX and DAPI fluorescence (as seen by the magenta colour) clearly indicates that pure DOX is co-localized in nucleus, whereas DOX-PSMN is mainly localized in the cytoplasm. This study demonstrates that the use of these nanoparticles as drug delivery vehicles could significantly enhance the accumulation of drug (DOX) in target cancer cells leading to a high therapeutic efficacy. We have also studied the cytotoxicity efficacy of DOX loaded PSMN in presence and absence of AMF (Fig. S8, ESI†). Due to the high loading efficiency of drug in the particles, substantial cell death is observed even in the absence of AMF. This makes it difficult to identify the combined effect of AMF and chemotherapy using present formulation, and cell viability experiments are needed in future at different drug levels to resolve the combinatorial effect. Further, the presence of polyaniline shell can improve the optical absorption of visible light of appropriate wavelength, depending on the structure of the polyaniline. The strong optical absorption of polyaniline can be exploited for laser induced heating of tumor cells as well. Towards this end, we performed thermal imaging experiments on solid PSMN after exposing to laser light of 532 nm. The infrared thermal images indicate local heating of particles by absorption of light and the temperature increases with an increase in exposure time (Fig. S9, ESI†).

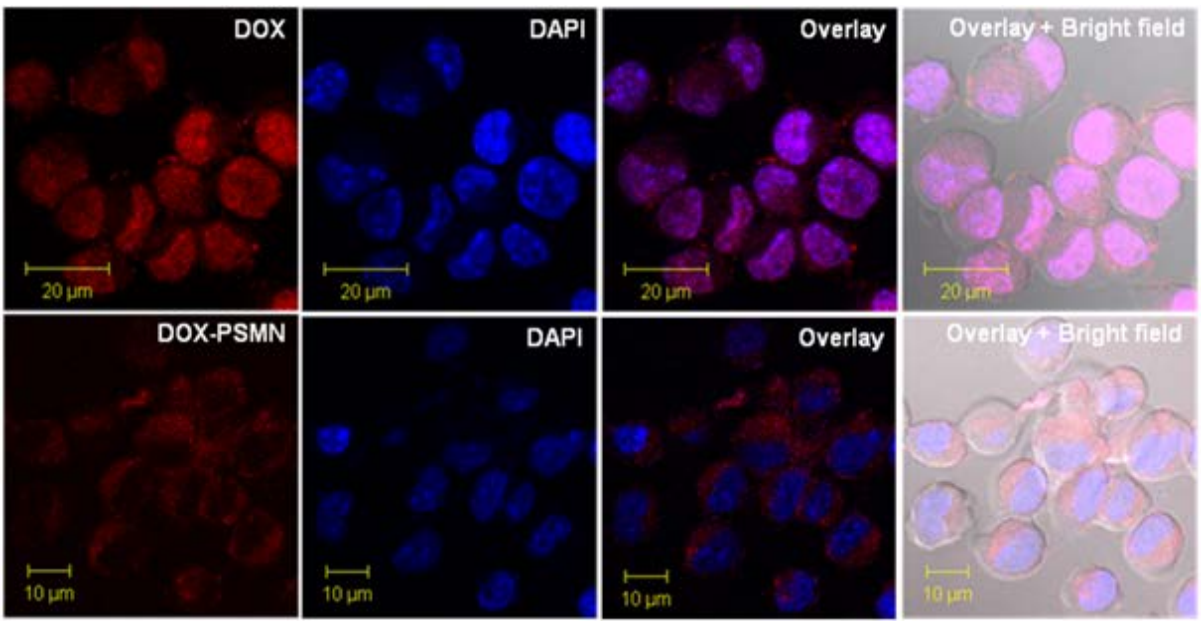


Fig. 9. CLSM images of WEHI-164 cells after incubation with the DOX, DOX-PSMN and DAPI at culture conditions (Top: pure DOX, Bottom: DOX-PSMN).

The magnetic hyperthermia, drug delivery and cellular internalization results of PSMN prompted us to explore their hemocompatibility and protein resistance characteristics for further *in-vivo* use. The hemocompatibility of PSMN was accessed by hemolysis assay and the percentage of hemolysis was found to be 3% upon incubation of 0.5 mg of PSMN. This low percentage of hemolysis (<5%) indicates the good hemocompatibility of PSMN. We also investigated the interaction of these nanoparticles with BSA protein at physiological medium (0.01 M PBS, pH 7.3). The PSMN do not show any significant change in zeta-potential (Table S1, ESI†) even after incubation with BSA for 2h, revealing their protein resistance characteristics at physiological medium. Specifically, our PSMN showed high drug (DOX) loading capacity, sustained drug release profile and excellent cellular internalization with good heating efficacy under AC magnetic field, which make the formulation with potential for the targeted drug delivery as well as hyperthermia treatment of cancer.

## Conclusions

Conducting polymer (polyaniline) impregnated shell cross-linked magnetic ($Fe_3O_4$) nanoparticles has been successfully prepared by a facile soft-chemical approach. The formation of single phase inverse spinel $Fe_3O_4$ nanoparticles of size about 10 nm is observed from XRD analysis and TEM micrograph. The FTIR spectra, DLS, TGA, zeta-potential and magnetic measurements clearly show the growth of polyaniline shell on the surface of carboxyl PEGylated $Fe_3O_4$ nanoparticles. These nanoparticles show good colloidal stability, high loading affinity for anticancer drug, sustained drug release profile, magnetic field induced heating, and substantial cellular internalization. It is interesting to mention that the polyaniline impregnated shell on PEGylated $Fe_3O_4$ nanoparticles enhances the heat activated killing of cancer cells under magnetic field. Taken together, the study suggests the prospective use of conducting polymer shell on magnetic nanoparticles for combinatorial cancer therapy involving hyperthermia and chemotherapy.

## Acknowledgment

Authors acknowledge Prof. D. Bahadur, Indian Institute of Technology Bombay, India for his encouragement, fruitful discussions and providing some experimental facilities. The authors also thank Mr. Manjoor Ali and Ms. Vasumathy Pillai for confocal laser scanning microscopy studies.

## References

1. M. Liong, J. Lu, M. Kovochich, T. Xia, S. G. Ruehm, A. E. Nel, F. Tamanoi and J. I. Zink, *ACS Nano*, 2008, **2**, 889.
2. X. F. Zhang, S. Mansouri, L. Clime, H. Q. Ly, L. H. Yahia and T. Veres, *J. Mater. Chem.*, 2012, **22**, 14450.
3. N. Kohler, C. Sun, A. Fichtenholtz, J. Gunn, C. Fang and M. Zhang, *Small*, 2006, **2**, 785.
4. A. Aqil, S. Vasseur, E. Duguet, C. Passirani, J. P. Benoît, R. Jérôme and C. Jérôme. *J. Mater. Chem.*, 2008, **18**, 3352.
5. K. C. Barick, S. Singh, D. Bahadur, M. A. Lawande, D. P. Patkar and P. A. Hassan, *J. Coll. Interf. Sci.*, 2014, **418**, 120.
6. J. Hu, Y. Qian, X. Wang, T. Liu and S. Liu, *Langmuir*, 2012, **28**, 2073.
7. M. Das, P. Dhak, S. Gupta, D. Mishra, T. K. Maiti, A. Basak and P. Pramanik, *Nanotechnol*., 2010, **21**, 125103.
8. D. -L. Zhao, H. -L. Zhang, X. -W. Zeng, Q. -S. Xia and J. -T. Tang, *Biomed Mater*., 2006, **1**, 198.
9. X. L. Liu, H. M. Fan, J. B. Yi, Y. Yang, E. S. G. Choo, J. M. Xue, D. D. Fan and J. Ding, *J. Mater. Chem.*, 2012, **22**, 8235.
10. V. M. Khot, A. B. Salunkhe, N. D. Thorat, R. S. Ningthoujam and S. H. Pawar, *Dalton Trans.*, 2013, **42**, 1249.
11. K. C. Barick and P. A. Hassan, *J. Coll. Interf. Sci.*, 2012, **369**, 96.
12. S. Mornet, S. Vasseur, F. Grasset and E. Duguet, *J. Mater. Chem.*, 2004, **14**, 2161.
13. K. C. Barick, M. Aslam, Y. P. Lin, D. Bahadur, P. V. Prasad and V. P. Dravid, *J. Mater. Chem.*, 2009, **19**, 7023.
14. K. C. Barick, S. Singh, N. V. Jadav, D. Bahadur, B. N. Pandey and P. A. Hassan, *Adv. Funct. Mater.*, 2012, **22**, 4975.
15. J. V. der Zee, *Ann. Oncol*., 2002, **13**, 1173.
16. . Bidan, O. Jarjayes, J. M. Fruchar and E. Hannecart, *Adv. Mater*., 1994, **6**, 152.
17. J. Deng, X. Ding, W. Zhang, Y. Peng, J. Wang, X. Long, P. Li and A.C. Chan, *Polymer*, 2002, **43**, 2179.
18. C. -L. Zhu, S. -W. Chou, S. -F. He, W. -N. Liao and C. -C. Chen, *Nanotechnol.*, 2007, **18**, 275604.
19. Q. Yu, M. Shi, Y. Cheng, M. Wang and H. -Z. Chen, *Nanotechnol.*, 2008, **19**, 265702.
20. B. Ding, S. Xia, K. Hayat and X. Zhang, *J. Agric. Food Chem.*, 2009, **57**, 2938.
21. C. Sun, K. Du, C. Fang, N. Bhattarai, O. Veiseh, F. Kievit, Z. Stephen, D. Lee, R. G. Ellenbogen, B. Ratner and M. Zhang, *ACS Nano*, 2010, **4**, 2402.
22. W. Lin, M. C. Garnett, E. Schacht, S. S. Davis and L. Illum, *Int. J. Pharm.*, 1999, **189**, 161.
23. J. Jang, J. Ha and B. Lim, *Chem. Commun.*, 2006, 1622.
24. J. Yin, X. Wang, R. Chang and X. Zhao, *Soft Matter*., 2012, **8**, 294.
25. B. González, E. Ruiz-Hernández, M. J. Feito, C. L. de Laorden, D. Arcos, C. Ramírez-Santillán, C. Matesanz, M. T. Portolés and M. Vallet-Regí, *J. Mater. Chem.*, 2011, **21**, 4598
26. M. Mikhaylova, D. Y. Kim, N. Bobrysheva, M. Osmolowsky, V. Semenov, T. Tsakalakos and M. Muhammed, *Langmuir*, 2004, **20**, 2472.
27. R. Ghosh, L. Pradhan, Y. P. Devi, S. S. Meena, R. Tewari, A. Kumar, S. Sharma, N. S. Gajbhiye, R. K. Vatsa, B. N. Pandey and R. S. Ningthoujam, *J. Mater. Chem.*, 2011, **21**, 13388.
28. B. Samanta, H. Yan, N. O. Fischer, J. Shi, D. J. Jerry and V. M. Rotello, *J. Mater. Chem.*, 2008, **18**, 1204.
29. M. Motskin, D. M. Wright, K. Muller, N. Kyle, T. G. Gard, A. E. Porter, J. N. Skepper, *Biomaterials*, 2009, **30**, 3307.
30. E. Munnier, F. Tewes, S. Cohen-Jonathan, C. Linassier, L. Douziech-Eyrolles, H. Marchais, M. Soucé, K. Hervé, P. Dubois and I. Chourpa, *Chem. Pharm. Bull.*, 2007, **55**, 1006.
31. F. A. D. Wolf, K. Nicolay and B. D. Kruijff, *Biochem.* 1992, **31**, 9252.
32. T. J. Higuchi, *J. Pharm. Sci.*, 1963, **52**, 1145.

# Polyaniline shell cross-linked $Fe_3O_4$ magnetic nanoparticles for heat activated killing of cancer cells

**Suman Rana,[a] Neena V. Jadhav,[b] K. C. Barick,*[,a] B. N. Pandey,[b] P. A. Hassan*[,a]**

[a]*Chemistry Division, Bhabha Atomic Research Centre, Mumbai-400085, India.*

[b]*Radiation Biology and Health Sciences Division, Bhabha Atomic Research Centre, Mumbai-400085, India*

Corresponding author: E-mail: kcbarick@barc.gov.in (K. C. Barick), hassan@barc.gov.in (P. A. Hassan); Fax: 91 22 2550 5151; Tel: 91 22 2559 5099

## Graphical abstract

Enhancement in heat activated killing of cancer cells under AC magnetic field using polyaniline shell cross-linked $Fe_3O_4$ magnetic nanoparticles.